nature communications

Article

https://doi.org/10.1038/s41467-024-52270-0

Coherent spin dynamics between electron and nucleus within a single atom

Received: 11 June 2024

Accepted: 30 August 2024

Published online: 11 September 2024

Check for updates

Lukas M. Veldman [1], Evert W. Stolte [1], Mark P. Canavan [1], Rik Broekhoven [1], Philip Willke [2], Laëtitia Farinacci [1] & Sander Otte [1]

The nuclear spin, being much more isolated from the environment than its electronic counterpart, presents opportunities for quantum experiments with prolonged coherence times. Electron spin resonance (ESR) combined with scanning tunnelling microscopy (STM) provides a bottom-up platform to study the fundamental properties of nuclear spins of single atoms on a surface. However, access to the time evolution of nuclear spins remained a challenge. Here, we present an experiment resolving the nanosecond coherent dynamics of a hyperfine-driven flip-flop interaction between the spin of an individual nucleus and that of an orbiting electron. We use the unique local controllability of the magnetic field emanating from the STM probe tip to bring the electron and nuclear spins in tune, as evidenced by a set of avoided level crossings in ESR-STM. Subsequently, we polarize both spins through scattering of tunnelling electrons and measure the resulting free evolution of the coupled spin system using a DC pump-probe scheme. The latter reveals a complex pattern of multiple interfering coherent oscillations, providing unique insight into hyperfine physics on a single atom level.

Nuclear spins have shown great promise as building blocks for quantum information in molecular spin qubits[1,2], NV centers[3,4], and donors in silicon[5]. They are also an excellent resource for quantum simulation[6], magnetic sensing[7,8] and spintronics[9], and are potentially scalable via engineered molecular and atomic networks[10,11]. Their key advantage arises from their longer coherence times compared to their electron spin counterpart[12], though the intricacies of the decoherence channels depend on the exact interaction with the environment which is hard to control in ensemble averaging techniques. Scanning tunneling microscopy (STM) constitutes an excellent means of investigation here, as it permits to address individual electron spins in electron spin resonance (ESR) experiments with sub-nanometer resolution[13,14], offering atomically precise information on their environment[15,16], and providing a pathway towards coherent control of the spins states[17,18]. In recent years, interactions involving the nuclear spin were measured indirectly by probing the hyperfine coupling in ESR-STM between the nucleus and the surrounding electrons[19]. In addition, the nuclear spin of individual Cu atoms could be polarized via spin pumping induced by the spin-polarized tunneling current[20]. However, accessing the coherent dynamics involving the nucleus remained challenging, due to its weak coupling to the tunneling electrons.

In this work, we show the free, coherent evolution between the nuclear spin and the electron spin in a single hydrogenated titanium atom. By fine-tuning the electronic Zeeman energy using the local field of the probe tip[21], we identify a parameter space where electronic and nuclear spin states hybridize. In a second step, we probe the free coherent evolution of the coupled system by electric DC pump-probe experiments[22]. Here, we reveal an emerging beating pattern, that originates from multiple quantum oscillations with different frequencies at the points of hybridization.

We use a commercial low-temperature STM equipped with high frequency cabling to send both RF signals and nanosecond DC pulses down to the tip. The sample system consists of Ti atoms deposited on bilayer MgO islands grown on Ag(100), that become hydrogenated by residual hydrogen[15,16]. For all measurements, we use spin-polarized tips

[1]Department of Quantum Nanoscience, Kavli Institute of Nanoscience, Delft University of Technology, Delft, The Netherlands. [2]Physikalisches Institut, Karlsruhe Institute of Technology, Karlsruhe, Germany. e-mail: a.f.otte@tudelft.nl

that are created by picking up co-deposited Fe atoms onto the tip apex. We study individual Ti adsorbed onto the oxygen sites of MgO – well-isolated from neighboring spins using atom manipulation (Fig. 1a) – which exhibit an effective electron spin $\hat{\boldsymbol{S}}$ with magnitude $S = ½$[15] and an anisotropic g-factor $\mathbf{g}$[16]. Throughout this work, we focus on ^{47}Ti isotopes, which carry a nuclear spin $\hat{\boldsymbol{I}}$ with magnitude $I = 5/2$. Along the principal axes of the crystal field (x,y,z, with z out of plane), the system is described by the following Hamiltonian:

$$\hat{\mathcal{H}} = \sum_{i=x,y,z} \left(\mu_B g_i \left(B_{\mathrm{ext},i} + B_{\mathrm{tip},i} \right) \hat{S}_i + A_i \hat{S}_i \hat{I}_i + Q_i \hat{I}_i^2 \right) \quad (1)$$

where μ_B is the Bohr magneton, and $\mathbf{A}$ and $\mathbf{Q}$ (see Supplementary Note 3)[19] are the hyperfine coupling and quadrupole contributions, respectively. The first term describes the Zeeman energy of the electron spin with contributions from both the external $\mathbf{B}_{\mathrm{ext}}$ and the tip-induced magnetic field $\mathbf{B}_{\mathrm{tip}}$. We neglect the effect of either of these fields on the nuclear spin, since their contributions are small compared to the other terms. In Fig. 1b we show the general behavior of the interplay between the hyperfine coupling and an external magnetic field. In the low field regime, the hyperfine coupling energy dominates and the system displays avoided crossings between the different energy levels indicating superposition states. In the high field regime, we retrieve the Zeeman spin states as eigenstates.

Results

State initialization via spin pumping

We start our investigation by applying a magnetic field of 1.5 T, which is large compared to the hyperfine interaction, in order to drive ESR transitions between the individual spin states of a ^{47}Ti atom. Similar to measurements of Ti on a bridge binding site of MgO[23,24], we find a large anisotropy in the hyperfine coupling $\mathbf{A} = [11, 11, 128] \pm 2$ MHz (see Supplementary Note 4 and Supplementary Fig. 3). Since we aim for a regime in which the hyperfine interaction competes with the Zeeman splitting of the electron, the experiments are performed with an out-of-plane magnetic field.

For certain magnetic tips (see Supplementary Note 1), we observe that the hyperfine-split ESR peaks have different intensities, which indicates a strong polarization of the nuclear spin. This effect is well known in bulk NMR techniques as hyperpolarization[25,26] and has been observed before on the atomic scale for single Cu atoms on MgO[20]. The phenomenon is explained by taking into account inelastic spin scattering events between the tunneling electrons and electron spin which are transmitted to the nucleus via the hyperfine flip-flop interaction. As shown in Fig. 1c, we find that the polarization is strongly dependent on the applied bias voltage while measuring at constant current. We believe that this may be due to the bias-dependent efficiency of the spin scattering channels involved, but a more complex mechanism involving the Ti orbital excitation[16] or Pauli spin blockade[27] may be at play. We find that the effective temperature of the nuclear spin population drops below 10 mK at voltages larger than 100 mV, more than two orders of magnitude lower than the actual experimental temperature of 1.5 K. While the effect of nuclear spin pumping has been observed for Cu on MgO, we here utilize it to overcome a major limitation: in previous ESR-STM experiments, the frequency ranges investigated were chosen to be compatible with sufficient spin population contrast set by the Boltzmann distribution at the experimental temperature. Finally,

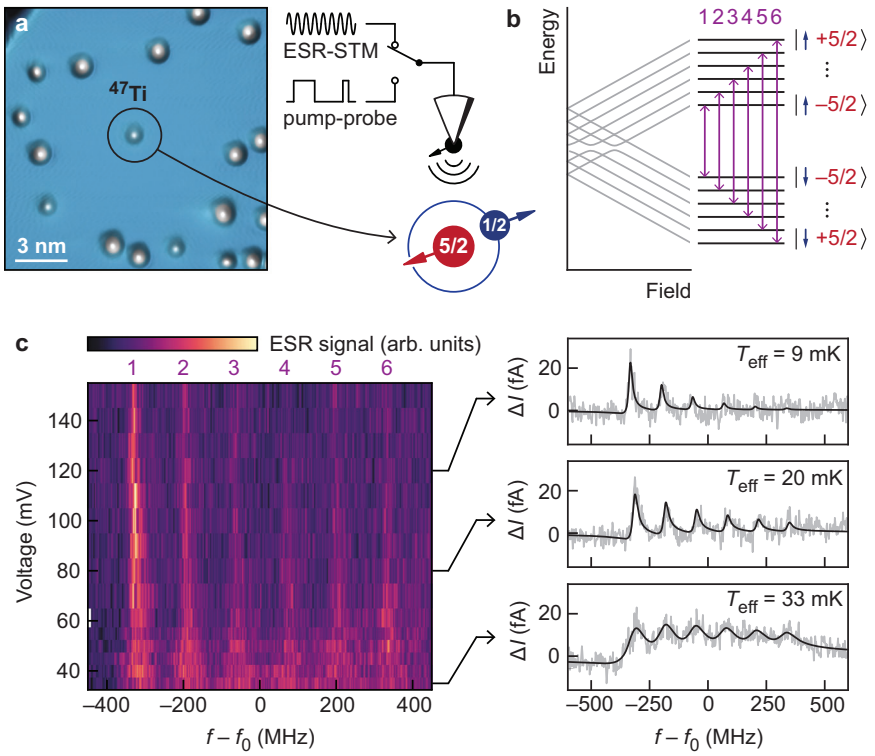

Fig. 1 | Single atom nuclear polarization. a STM topography of the single ^{47}Ti studied in this work. A schematic drawing shows the magnetic STM tip above the electron spin (blue) and nuclear spin (red) of the single atom. **b** Energy diagram of the spin states of a single ^{47}Ti. In the low field regime, avoided crossings appear between the different eigenstates. In the high field regime, the eigenstates resemble Zeeman product states. ESR transitions (purple arrows) can be driven between states with equal nuclear spin. **c** ESR-STM measurements at different applied DC bias ($T = 1.5$ K, $B_{\mathrm{ext}} = 1.5$ T, $V_{\mathrm{RF}} = 25$ mV, $I_{\mathrm{set}} = 2.5$ pA, $f_0 = 11.5$–12.56 GHz). The observed variation in resonance frequency f_0 likely results from a combination of the tip field changing with tip height and a voltage dependence of the resonance[28]. Line traces at 35 mV, 80 mV, and 120 mV are shown with fits using six Fano lineshapes scaled by the Boltzmann factor in order to extract an effective temperature.

https://doi.org/10.1038/s41467-024-52270-0

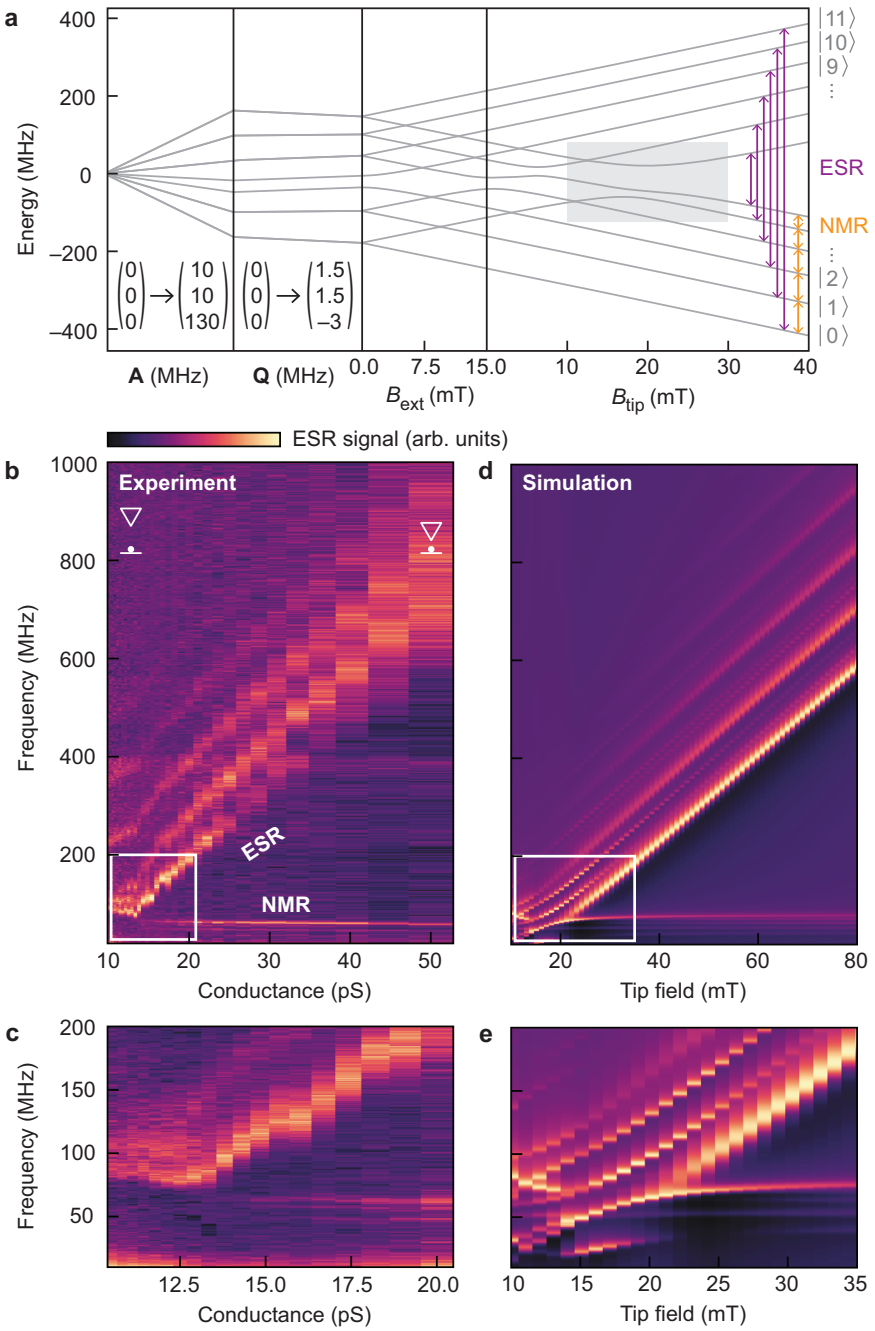

Fig. 2 | ESR and NMR-type measurements in the low-field regime. a Energy diagram of the atomic eigenstates as a function of hyperfine coupling, quadrupole moment, external and tip-induced magnetic field. For details on the calculations of the eigenstates, see Supplementary Note 3. **b** ESR-STM measurements ($T = 400$ mK, $B_{ext} = 20$ mT, $V_{RF} = 40$ mV, $I_{set} = 2$ pA, $V_{set} = 40$–200 mV) as function of tip-sample conductance. As indicated with icons, tip-sample separation decreases towards the right side of the plot, corresponding to an increasing tip-induced magnetic field. Both ESR and NMR-type transitions are observed and indicated as such. The bottom close-up is a separate dataset showing the splitting of the NMR transitions and a curve upwards of the bottom ESR transition signaling the avoided level crossing. Each trace is normalized and the average value is subtracted in order to compensate for the bias-dependent rectification current. **c** Separate ESR dataset ($T = 400$ mK, $B_{ext} = 20$ mT, $V_{RF} = 40$ mV, $I_{set} = 2$ pA, $V_{set} = 100$–190 mV) zoomed in to marked region of (**b**). **d** Simulations of the ESR-STM measurements (see Methods), where we consider the tip field to make an 8° angle with the out-of-plane external field. **e** Zoom-in to marked region of (**d**).

we point out that high bias voltages are key for efficient nuclear spin pumping, which – with few exceptions[28] – has usually not been used in previous experiments involving Ti on MgO.

Tuning electron-nuclear spin entanglement

Owing to the spin pumping we can investigate a much lower frequency regime, down to ~50 MHz, in which the level of entanglement between the electron and nuclear spins can be tuned. In Fig. 2a, we show the different calculated contributions to the energy diagram of a ^{47}Ti in a low-field regime. For the calculations we use $\mathbf{A} = [10,10,130]$ MHz and $\mathbf{Q} = [1.5,1.5,-3]$ MHz in accordance with the measurements performed in a vector field (see Supplementary Note 3). When the total electronic Zeeman energy – due to the external and tip magnetic field – is comparable to the hyperfine splitting, multiple avoided level crossings occur in the spectrum. The number of avoided crossings has increased compared to Fig. 1b which is due to a misalignment between the external

https://doi.org/10.1038/s41467-024-52270-0

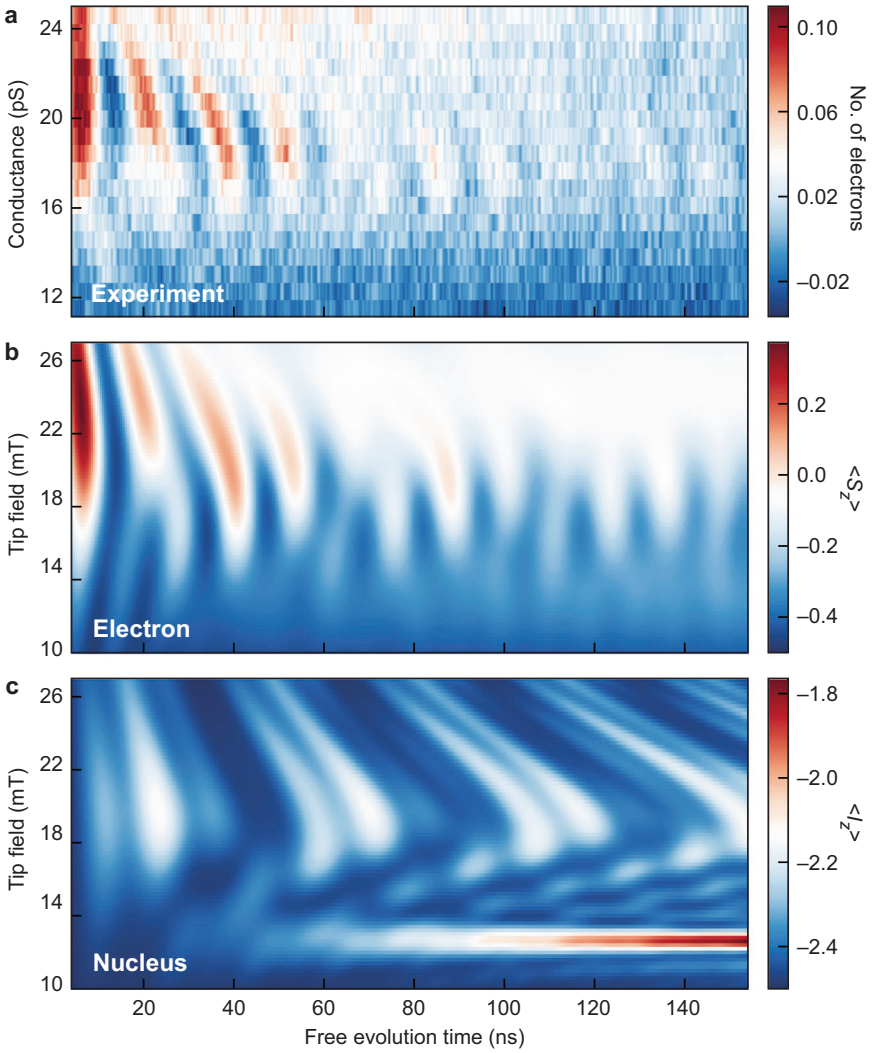

Fig. 3 | Free evolution measurements and Lindblad simulations. a Pump-probe data for different tip-atom distances set by the junction conductance (V_{set} = 130 mV, T = 400 mK, B = 15 mT, for details on the pulse scheme, see Supplementary Note 7). **b** Liouville-von Neumann simulation of the free time evolution of the electron spin when initialized to $|\downarrow, -5/2\rangle$. Simulation is convolved with a 2 mT Gaussian in the tip-field axis to simulate level broadening due to mechanical vibrations of the tip. **c** Corresponding simulation of the free time evolution of the nuclear spin, revealing the observed electron spin oscillations being accompanied by nuclear spin fluctuations. The calculations also show the onset of an additional oscillation in the nuclear spin at ~13 mT. However, since the period is an order of magnitude longer than the coherence time of the electron spin, it is not visible in our measurements.

field and the tip field. More precisely, an additional avoided crossing appears around B_{tip} = 23 mT, involving a superposition of states that differ only in the electron spin projection, while the nuclear spin is the same. This electron-only hybridization will be of importance below.

We identify these tuning points in our experiment by performing ESR measurements in the low field regime using an external field of merely 20 mT (Fig. 2b). Here, in order to fine-tune the coupled spin system, we vary the tip-induced magnetic field by changing the DC voltage while keeping the current constant. This effectively tunes the junction conductance G. At relatively large tip fields ($G \geq 20$ pS) multiple ESR peaks are visible in addition to several very sharp (~3 MHz) NMR type resonances around 60 MHz. Below $G \approx 20$ pS, the ESR and NMR transitions start to mix and overlap, accompanied by a redistribution of their intensities as shown in the close-up measurements in Fig. 2c. This is consistent with the presence of avoided level crossings between the energy levels, as expected from Fig. 2a and modeled in Fig. 2d, e. In Fig. 2c, we also observe that the NMR type resonances are split into multiple peaks. We attribute this to the quadrupole interaction that slightly shifts the energy of each nuclear spin state[19]. For the simulations we consider both ESR and NMR transitions with separately scaled intensities (see Supplementary Note 5).

Probing coherent spin dynamics

Having identified 10–20 pS as the appropriate tip-atom distances for inducing superposition states, we perform DC pump-probe experiments to explore the coupled spin dynamics. In order to increase signal amplitudes, we decrease the external field to 15 mT so that the superposition states are induced at closer tip-atom distances while using the same microtip. We use a two-pulse pumping sequence (see Supplementary Note 6 and Supplementary Fig. 4) to initialize both electron and nuclear spin states. During the pump pulses, spin-polarized electrons cause spin-flip excitations in the atom by scattering with the atom's electron spin[29]. Due to the hyperfine coupling, the excitations will also affect the nuclear spin, polarizing it in the same direction[20]. Consequently, the combined system will be projected to a Zeeman state, $|\downarrow, -5/2\rangle$ which is not necessarily a stationary eigenstate of the Hamiltonian of Eq. (1). To probe any dynamics that might occur after the pump pulses, we then let the system evolve freely during a waiting time after which the electron spin is read out by a 5 ns

https://doi.org/10.1038/s41467-024-52270-0

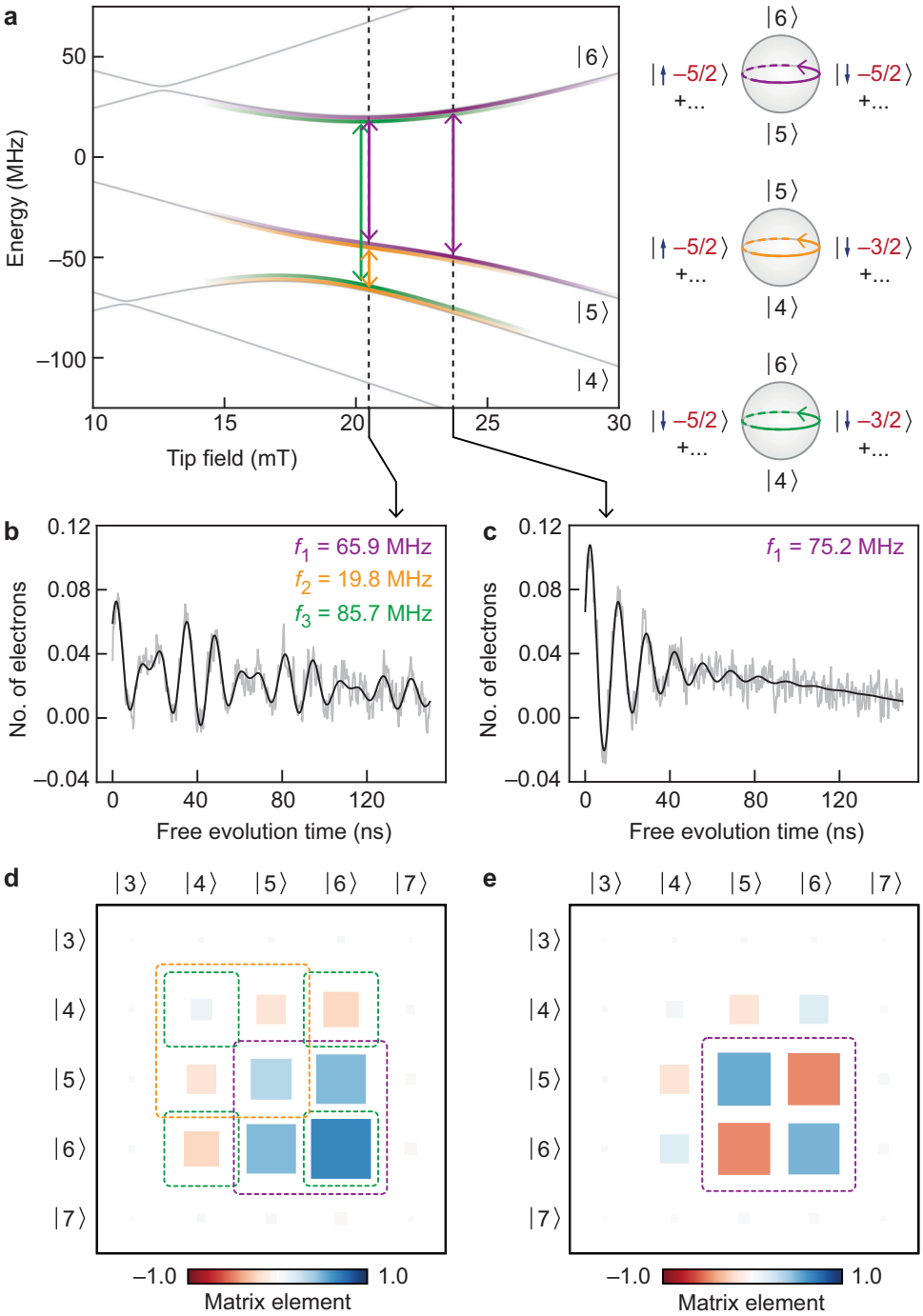

Fig. 4 | Origin of the beating pattern. a Zoom-in on the relevant avoided level crossings of Fig. 2a. The Bloch spheres illustrate the dominating dynamics arising from the superpositions of the corresponding states. **b** Fit to a line trace from the pump-probe data from Fig. 3a showing a beating pattern ($G = 17.7$ pS). The pattern arises from two dominating frequencies and their sum frequency. **c** Fit to a line trace from the pump-probe data from Fig. 3a showing a single frequency oscillation ($G = 21.5$ pS). **d** Reduced density matrix of the initial state $|\downarrow, -5/2\rangle$ at 20.5 mT tip field. **e** Reduced density matrix of the initial state $|\downarrow, -5/2\rangle$ at 23.7 mT tip field.

probe pulse. By varying the waiting time over the course of many iterations, the dynamic evolution of the electron spin is measured[8].

Using this pulse scheme we observe electron spin dynamics that, as shown in Fig. 3a, depend on the tip magnetic field. When the STM tip is close (i.e., at large conductance values) we observe fast, low-amplitude oscillations that become slower and stronger as the tip is retracted. This is the expected behavior when the system moves through an avoided crossing[22]. However, near $G = 17$ pS a beating pattern appears due to interference with a second frequency. At this point, the dynamics also appear to be longer lived compared to the single-frequency oscillation. Upon further retraction of the tip, below $G = 15$ pS, no spin dynamics are detected anymore. The observed dynamics occur at slightly higher conductance values compared to the detected avoided crossing measured using ESR in Fig. 2. We attribute this difference to both the slightly lower external field used for the pump-probe measurements as well as the absence of a DC bias voltage in the pump-probe experiment, which has been shown to shift the electron energy levels[28].

Figure 3b, c show the simulated time evolution of the S_z and I_z expectation values for the electron and the nuclear spin,

respectively. The calculations are performed considering the Hamiltonian shown in Eq. (1) and using the Liouville-von Neumann equation starting from the $|\downarrow, -5/2\rangle$ state[30]. We find excellent agreement between the data from the experiment and the electronic spin calculations, with, in particular, a beating pattern that arises when the electron and nucleus states are entangled. While the electron shows an interference pattern, the simulation shows that the dynamics of the nuclear spin are dominated by an oscillation with approximate period 40 ns.

To understand the origin of the different oscillations, we further analyze the composition of the three states forming the avoided crossings: energy eigenstates $|4\rangle$, $|5\rangle$ and $|6\rangle$. In Fig. 4a, we show an enhanced view of the relevant region of the eigenstate energies marked by the gray box in Fig. 2a. We then take two exemplary traces from the pump-probe data presented in Fig. 3a and match the frequencies present in the spin dynamics to the energy splitting between the eigenstates. From the composition of the eigenstates at these particular tip-field amplitudes we derive the nature of the different dynamics (see Supplementary Note 3).

At a relatively large setpoint conductance of 21.5 pS, the pump-probe data fitted in Fig. 4c show a single damped sinusoid of roughly 75 MHz. This frequency matches both the energy of the lowest ESR transition measured at the avoided crossing point in Fig. 2b as well as the calculated energy splitting between states $|5\rangle$ and $|6\rangle$ at the relatively large tip field of roughly 24 mT (rightmost dotted line in Fig. 4a). At this field, states $|5\rangle$ and $|6\rangle$ are split in energy by the in-plane component of the tip field and approximate the spin superposition states $|\uparrow, -5/2\rangle \pm |\downarrow, -5/2\rangle$ (see Supplementary Fig. 2). Therefore, the reduced density matrix of the initial state $|\downarrow, -5/2\rangle$, shown in Fig. 4e, is dominated by coherences in the subspace between states $|5\rangle$ and $|6\rangle$. We can thus attribute the dominant frequency in the dynamics to a Larmor precession of the electron spin due to the in-plane component of the tip field as depicted in the top Bloch sphere in Fig. 4a.

In contrast, at a setpoint conductance of 17.7 pS, we need three damped sinusoids to fit the data shown in Fig. 4b: two independent frequencies, 65.9 MHz and 19.8 MHz as well as their sum. These frequencies match the energy splitting between the three states $|4\rangle$, $|5\rangle$ and $|6\rangle$ at roughly 20 mT (leftmost dotted line in Fig. 4a). The reduced density matrix of the initial state at this field, shown in Fig. 4d, show finite coherences between all three states. This means that in addition to the Larmor contribution described above, there are two additional terms. One is a flip-flop dynamic between electron and nucleus as the subspace between states $|4\rangle$ and $|5\rangle$ is dominated by $|\uparrow, -5/2\rangle \pm |\downarrow, -3/2\rangle$ (middle Bloch sphere in Fig. 4a). The other is an oscillation of the nuclear spin as the subspace between states $|4\rangle$ and $|6\rangle$ is dominated by $|\downarrow, -5/2\rangle \pm |\downarrow, -3/2\rangle$ (bottom Bloch sphere in Fig. 4a).

The reduced coupling of the nuclear spin to the environment, compared to the dynamics of only the electron spin, is expected to result in an enhanced coherence time[8,31,32]. Indeed, fits to the data shown in Fig. 4b result in an effective coherence time of 84 ± 5 ns, whereas the oscillation in Fig. 4c has an effective coherence time of only 22 ± 1 ns. However, we point out that this is only a lower limit to the intrinsic coherence time of the combined electron-nucleus spin system. We believe that the main source of spin decoherence in our experiment is fluctuations of the magnetic field emanating from the tip caused by mechanical vibrations in the setup on the sub-picometer scale. The observed changes in coherence time may in part result from a decreased sensitivity to this magnetic tip field noise since the energy levels in Fig. 4a diverge less at 21 mT than at 23 mT, akin to a clock-transition[33,34]. We expect that eliminating these vibrations may result in longer coherence times in pump-probe measurements.

Discussion

Developing single-atom quantum information processing requires thorough understanding of the underlying electron and nuclear spin dynamics. This demands initialization, tuning and readout tailored on the atomic length scale. Using pump-probe spectroscopy, we revealed the collective coherent dynamics of the internal spin dynamics inside a single atom. The magnetized STM tip functioned in this work as a control knob to locally tune the nature of these dynamics. This technique has the potential to be extended to a great variety of on-surface atomic or molecular spin system. Moreover, the prospect of STM for engineering bottom-up atomic designer assemblies can provide an integral atomic-scale understanding into the fundamentals of complex coherent spin dynamics.

Methods

Extended information on used methods is provided in Supplementary Information.

Data availability

The raw data generated in this study as well as the analysis and simulation code have been deposited in a Zenodo database under identifier https://doi.org/10.5281/zenodo.8316339.

References

1. Vincent, R., Klyatskaya, S., Ruben, M., Wernsdorfer, W. & Balestro, F. Electronic read-out of a single nuclear spin using a molecular spin transistor. *Nature* **488**, 357–360, (2012).
2. Thiele, S. et al. Electrically driven nuclear spin resonance in single-molecule magnets. *Science* **344**, 1135–1138 (2014).
3. Neumann, P. et al. Single-shot readout of a single nuclear spin. *Science* **329**, 542–544 (2010).
4. Fuchs, G. D., Burkard, G., Klimov, P. V. & Awschalom, D. D. A quantum memory intrinsic to single nitrogen-vacancy centres in diamond. *Nat. Phys.* **7**, 789–793 (2011).
5. Pla, J. J. et al. High-fidelity readout and control of a nuclear spin qubit in silicon. *Nature* **496**, 334–338 (2013).
6. Randall, J. et al. Many-body-localized discrete time crystal with a programmable spin-based quantum simulator. *Science* **374**, 1474–1478 (2021).
7. Maze, J. R. et al. Nanoscale magnetic sensing with an individual electronic spin in diamond. *Nature* **455**, 644–647 (2008).
8. Zaiser, S. et al. Enhancing quantum sensing sensitivity by a quantum memory. *Nat. Commun.* **7**, 12279 (2016).
9. Zutic, I., Fabian, J. & Das Sarma, S. Spintronics: fundamentals and applications. *Rev. Mod. Phys.* **76**, 323–410 (2004).
10. Wernsdorfer, W. & Ruben, M. Synthetic hilbert space engineering of molecular qudits: isotopologue chemistry. *Adv. Mater.* **31**, 1806687 (2019).
11. Kane, B. E. A silicon-based nuclear spin quantum computer. *Nature* **393**, 133–137 (1998).
12. Yang, S. et al. High-fidelity transfer and storage of photon states in a single nuclear spin. *Nat. Photon.* **10**, 507–511 (2016).
13. Baumann, S. et al. Electron paramagnetic resonance of individual atoms on a surface. *Science* **350**, 417–420 (2015).
14. Willke, P., Yang, K., Bae, Y., Heinrich, A. J. & Lutz, C. P. Magnetic resonance imaging of single atoms on a surface. *Nat. Phys.* **15**, 1005–1010 (2019).
15. Yang, K. et al. Engineering the eigenstates of coupled spin-1/2 atoms on a surface. *Phys. Rev. Lett.* **119**, 227206 (2017).
16. Steinbrecher, M. et al. Quantifying the interplay between fine structure and geometry of an individual molecule on a surface. *Phys. Rev. B* **103**, 155405 (2021).
17. Yang, K. et al. Coherent spin manipulation of individual atoms on a surface. *Science* **366**, 509–512 (2019).

18. Wang, Y. et al. Universal quantum control of an atomic spin qubit on a surface. *Npj Quant. Inf.* **9**, 48 (2023).
19. Willke, P. et al. Hyperfine interaction of individual atoms on a surface. *Science* **362**, 336–339 (2018).
20. Yang, K. et al. Electrically controlled nuclear polarization of individual atoms. *Nat. Nanotechnol.* **13**, 1120–1125 (2018).
21. Yang, K. et al. Tuning the exchange bias on a single atom from 1 mT to 10 T. *Phys. Rev. Lett.* **122**, 227203 (2019).
22. Veldman, L. M. et al. Free coherent evolution of a coupled atomic spin system initialized by electron scattering. *Science* **372**, 964–968 (2021).
23. Farinacci, L., Veldman, L. M., Willke, P. & Otte, S. Experimental determination of a single atom ground state orbital through hyperfine anisotropy. *Nano Lett.* **22**, 8470–8474 (2022).
24. Kim, J. et al. Anisotropic hyperfine interaction of surface-adsorbed single atoms. *Nano Lett.* **22**, 9766–9772 (2022).
25. Cassidy, M. C., Chan, H. R., Ross, B. D., Bhattacharya, P. K. & Marcus, C. M. In vivo magnetic resonance imaging of hyperpolarized silicon particles. *Nat. Nanotechnol.* **8**, 363–368, (2013).
26. Eills, J. et al. Spin hyperpolarization in modern magnetic resonance. *Chem. Rev.* **123**, 1417–1551 (2023).
27. McMillan, S. R., Harmon, N. J. & Flatte, M. E. Image of dynamic local exchange interactions in the dc magnetoresistance of spin-polarized current through a dopant. *Phys. Rev. Lett.* **125**, 257203 (2020).
28. Kot, P. et al. Electric control of spin transitions at the atomic scale. *Nat. Commun.* **14**, 6612 (2023).
29. Loth, S., Etzkorn, M., Lutz, C. P., Eigler, D. M. & Heinrich, A. J. Measurement of fast electron spin relaxation times with atomic resolution. *Science* **329**, 1628–1630, (2010).
30. Johansson, J. R., Nation, P. D. & Nori, F. QuTiP: an open-source Python framework for the dynamics of open quantum systems. *Comput. Phys. Commun.* **183**, 1760–1772 (2012).
31. Degen, C. L., Reinhard, F. & Cappellaro, P. Quantum sensing. *Rev. Mod. Phys.* **89**, 035002 (2017).
32. Savytskyy, R. et al. An electrically driven single-atom "flip-flop" qubit. *Sci. Adv.* **9**, eadd9408 (2023).
33. Bae, Y. et al. Enhanced quantum coherence in exchange coupled spins via singlet-triplet transitions. *Sci. Adv.* **4**, eaau4159 (2018).
34. Shiddiq, M. et al. Enhancing coherence in molecular spin qubits via atomic clock transitions. *Nature* **531**, 348–351 (2016).

Acknowledgements

This work was supported by the Dutch Research Council (NWO Vici Grant VI.C.182.016) and by the European Research Council (ERC Advanced Grant No. 101095574 "HYPSTER"). P.W. acknowledges funding from the Emmy Noether Programme of the DFG (WI5486/1-1) and the Daimler and Benz Foundation.

Author contributions

L.M.V., L.F., and S.O. conceived the experiment. L.M.V., M.P.C., and E.W.S. performed the measurements. L.M.V., M.P.C., and R.B. performed the calculations. All authors analyzed and discussed the results. L.M.V., L.F., P.W., and S.O. wrote the manuscript, with input from all authors. S.O. supervised the project.

Competing interests

The authors declare no competing interests.

Additional information

Supplementary information The online version contains supplementary material available at https://doi.org/10.1038/s41467-024-52270-0.

Correspondence and requests for materials should be addressed to Sander Otte.

Peer review information *Nature Communications* thanks the anonymous reviewers for their contribution to the peer review of this work. A peer review file is available.